

Supporting Information

A Mixed-valence $(\text{Fe}^{\text{II}})_2(\text{Fe}^{\text{III}})_2$ Square for Molecular Expression of Quantum Cellular Automata

*Yonggang Zhao, Dong Guo, Yang Liu, Cheng He and Chunying Duan**

Experimental Section

Figure S1. Electrospray mass spectrum of $1 \cdot (\text{ClO}_4)_2 \cdot (\text{H}_2\text{O})$

Figure S2. Magnetic susceptibility data

Figure S3. Variation in the IVCT peak maxima with solvent polarity

Explanation the splitting of the IT bands

Experimental Section

Materials and Methods. All chemicals were of reagent grade quality obtained from commercial sources and used without further purification. The elemental analyses of C, H and N were performed on a Perkin-Elmer 240C elemental analyzer. Electrospray mass spectra were carried out on a LCQ system (Finnigan MAT, USA) using methanol as mobile phase. UV-vis-NIR spectra were measured at room temperature on a Shimmadzu 3100 spectrophotometer in CD₃CN or CH₃CN solution for compound **1**·(ClO₄)₂·(H₂O) and other compounds, respectively. Cyclic voltammetry (CV) measurements were carried out on a BAS 100W system in a three-electrode cell with a pure Ar gas inlet and outlet. These experiments were carried out with a 1 × 10⁻³ M solution of compound **1**·(ClO₄)₂·(H₂O) in CH₃CN containing 0.1 M of (n-C₄H₉)₄NClO₄ as electrolyte. The potentials quoted in this work were relative to an Ag/AgCl electrode with a glassy carbon electrode as a working electrode.

Compound 1·(ClO₄)₂·(H₂O) FeSO₄·7H₂O (0.028g, 0.1mmol) and ligand H₂L (bis[phenyl(2-pyridyl)methanone]thiocarbazone)^[23] (0.044g, 0.1mmol) were mixed in absolute methanol (20ml). After refluxing for 1h, and cooling to room temperature, NaClO₄ (0.028g, 0.2mmol) was added and refluxing was resumed for 3hrs. The dark-green crystals suitable for X-ray structural determination were obtained by evaporation a methanol solution in air. Anal. Calcd. for Fe₄C₁₀₀H₇₄N₂₄S₄Cl₂O₉: C, 55.1; H, 3.4; N, 15.4; Found: C, 54.9; H, 3.6; N, 15.2; ESI-MS: *m/z* 980.6, ([Fe₄L₄]²⁺); IR (KBr, cm⁻¹): ν 1328m, 1304m, 1276w (C=S).

Crystallography X-Ray intensity data were measured at 180(2) K on a Bruker SMART APEX CCD-based diffractometer (Mo-Kα radiation, $\lambda = 0.71073 \text{ \AA}$) using the SMART and SAINT programs. The structures were solved by direct methods and refined on F^2 by full-matrix least-squares methods with SHELXTL version 5.1. All of the non-hydrogen atoms except the several were refined with anisotropic thermal displacement coefficients. Hydrogen atoms were located geometrically and refined in a riding model. To assist the refinements, several restraints were applied: (1) the S atoms, one of the phenyl rings and the O atoms of the perchloride ion were disordered into two parts with the site occupancy factors of the atoms being refined by free variable; (2) the geometrical constraints of idealized regular

polygons and polyhedrons for the phenyl rings and the anion were used, such as the Cl–O distance being 1.430 Å and the C–C distance of the phenyl ring being 1.395 Å, the C–S distances for the two disordered parts of the S atoms were refined to be same; (3) thermal parameters on adjacent atoms in the anion and the phenyl moieties were restrained to be similar.

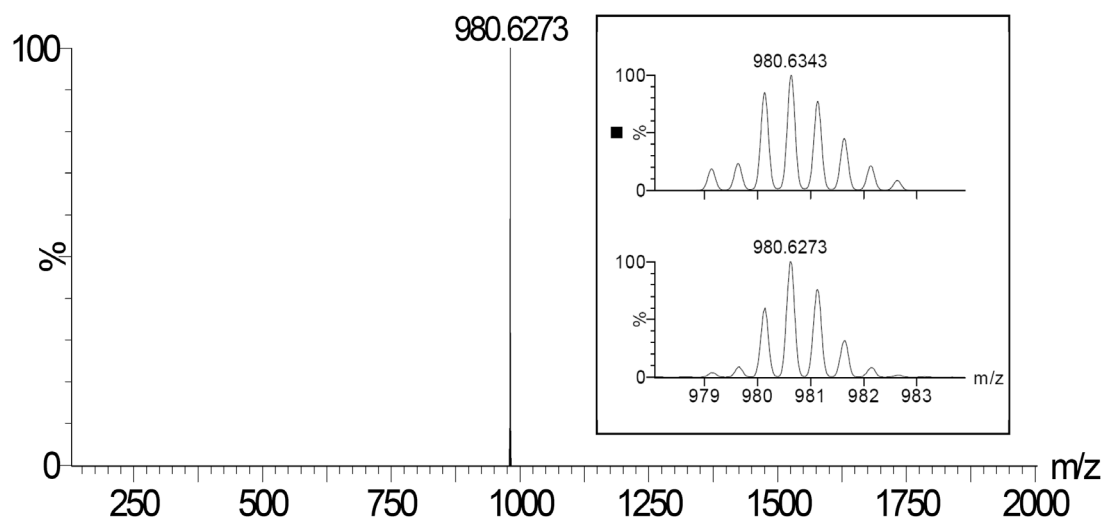


Figure S1. Electrospray mass spectrum of $\mathbf{1}\cdot(\text{ClO}_4)_2\cdot(\text{H}_2\text{O})$ in an acetonitrile solution.

The insert pictures exhibit the high-resolution spectrum (the bottom picture) and the simulation pattern of the expected species (the top picture).

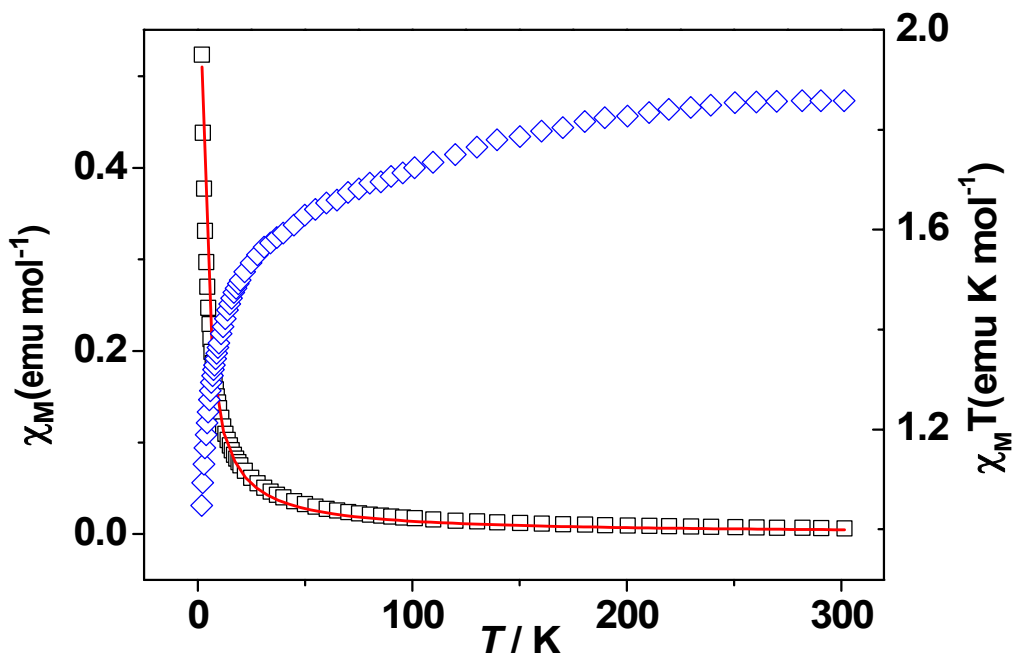


Figure S2. Magnetic susceptibility data χ_M (black) and $\chi_M T$ (blue) as functions of temperature for compound **1**·(ClO₄)₂·(H₂O). The red solid line represents the best fit to the model of the two S = ½ centers.

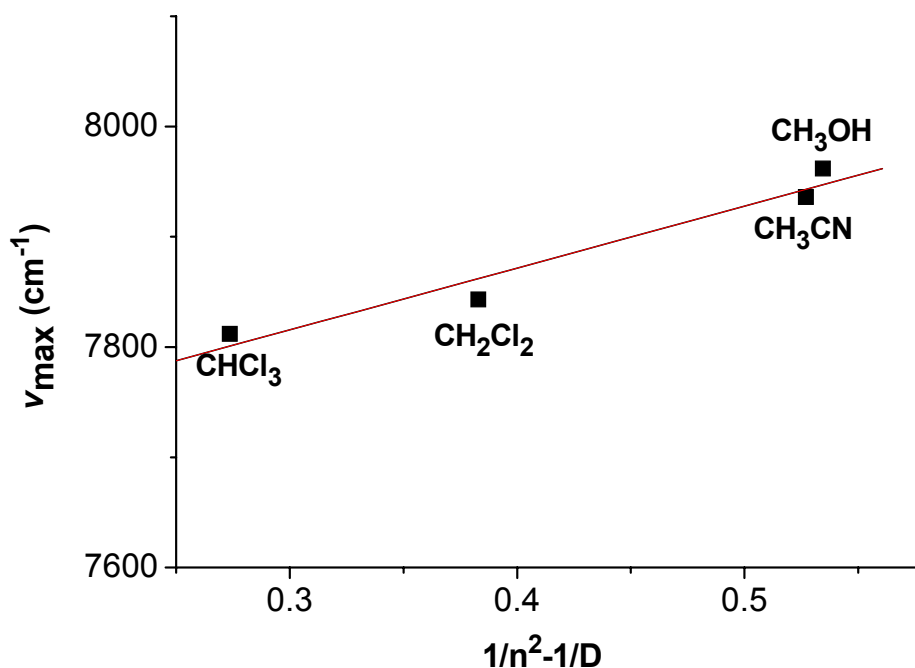


Figure S3. Variation in the IVCT peak maxima with solvent polarity for compound **1**·(ClO₄)₂·(H₂O), in where n is the optical dielectric constant and D is the static dielectric constant of the solvent, respectively.

Explanation the splitting of the IT bands

By applying a multidimensional electron transfer theory developed by Lambert, the six diabatic states (A-B-C) of $\mathbf{1}^{2+}$ are shown in **Figure S4**. While four of the diabatic states (B) have the same energy, the other two states (A and C) are at lower energy due to electrostatic repulsion. The electrons (or holes) at opposite corners of the square are set as A and C, while they are adjacent as B. By using Lambert's methodology, the set of diabatic (noninteracting) states, which were coupled by the multidimensional Mulliken-Hush formula, is given in **Figure S4**. The high energy excited states that have no direct coupling from the ground state into these states are omitted, because the transition forbidden will only result in very weak IVCT bands at much higher energy than the IVCT band observed. The meta coupling V_2 between such as diabatic states B_1 and B_2 is also set to zero, because it is expected to be much smaller than V owing to the meta conjugation path. Having performed these simplifications, the determinant, in which only the diabatic states A(C) coupled with B is shown in **Equation S1**.

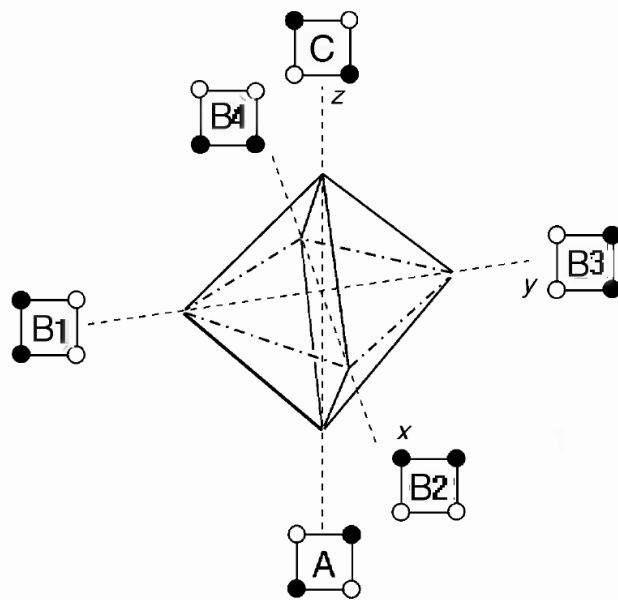


Figure S4 Diagram of the six diabatic states and their ET pathways. The full circles of the square symbols refer to oxidised redox sites while the open circles refer to reduced sites. The edges of the octahedron refer to single-electron transfer pathways given by the coupling V_1 (—) and V_2 (•—). The x , y and z coordinates refer to two-electron transfer pathways with $V = 0$. The origin of the coordinate system is in the centre of the octahedron, the corners are placed at $\pm \sqrt{2}/2$.

$$\begin{array}{ccccccc}
 \lambda(x^2+y^2+\frac{\sqrt{2}}{2}z^2)-\varepsilon & V_1 & V_1 & V_1 & V_1 & 0 & \\
 V_1 & \lambda(x^2+(\frac{\sqrt{2}}{2}+y)^2+z^2)+\Delta G-\varepsilon & V_2 & 0 & V_2 & V_1 & \\
 V_1 & V_2 & \lambda(\frac{\sqrt{2}}{2}+x^2+y^2+z^2)+\Delta G-\varepsilon & V_2 & 0 & V_1 & \\
 V_1 & 0 & V_2 & \lambda(x^2+(\frac{\sqrt{2}}{2}-y)^2+z^2)+\Delta G-\varepsilon & V_2 & V_1 & \\
 V_1 & V_2 & 0 & V_2 & \lambda(\frac{\sqrt{2}}{2}-x^2+y^2+z)+\Delta G-\varepsilon & V_1 & \\
 0 & V_1 & V_1 & V_1 & V_1 & \lambda(x^2+y^2+(\frac{\sqrt{2}}{2}-z^2)-\varepsilon & \\
 \end{array} = 0 \quad (1)$$

* The Figure and the Equation were copied from the ref: C. Lambert, *Chemphyschem*, 2003, 4, 877–880.

Where ΔG° is the net energy difference between the potentials of the two Fe^{III} at diagonal positions and at *ortho* positions that mainly arises from the electrostatic repulsion potential and potential magnetic interactions; λ is the diabatic potential corresponding to the each diabatic states. Diagonalisation of the matrix in the Equation S1 yields the adiabatic ground state (A_{1g} in the delocalized D_{4h} case) and five excited states (T_u , B_{1g} , A_{1u}). Consequently, the lower energy IVCT is likely to

correspond to the single electron transition from the ground state A_{1g} to the first excited state B_{1g} , and the high energy IVCT to the single electron transition from the ground state A_{1g} to the second excited state T_u , whereas the two-electron transition between the ground state and the highest excited state A_{1u} is always forbidden.

In the case of the valence delocalized complex $\mathbf{1}^{2+}$, the diabatic potential (λ) is much smaller than that of electron coupling potential V . The energy difference between the lower energy IVCT (v_1) and the higher energy IVCT (v_2) should be equal to the energy difference ΔG° (2320 cm^{-1}), and the energy of the forbidden two-electron transition might be the energy summation of the two single-electron transitions. Whereas the electron coupling potential V is determined by using $(v_1 v_2 / 8)^{1/2}$ as 2350 cm^{-1} , the ground state thus comprises of these six diabatic states with the occupation probability being calculated as $\frac{1}{2}v_2/(v_2 + v_1)$ for diabatic states A and C, $\frac{1}{4}v_1/(v_2 + v_1)$ for diabatic states B_1 , B_2 , B_3 and B_4 , respectively. The energy minimum of the ground state is at the point that diabatic states A or C occupied.

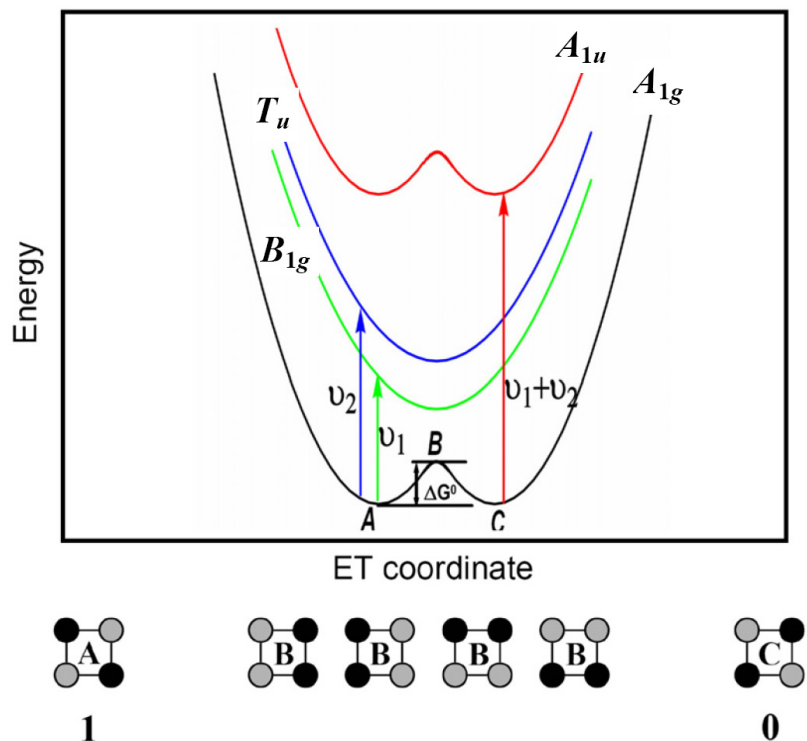


Figure S4. Schematic two-well potential illustrating the tunable barriers induced by the presence of the intermediate states with two excess electrons sited in one edge of the molecular square. The black balls represent the Fe^{II} centers, while the gray balls show the Fe^{III} centers.